Inorganic Chemistry

Article

pubs.acs.org/IC

L-Tyrosinatonickel(II) Complex: Synthesis and Structural, Spectroscopic, Magnetic, and Biological Properties of 2{[Ni(L-Tyr)$_2$(bpy)]}·3H$_2$O·CH$_3$OH

Agnieszka Wojciechowska,*[,†] Anna Gągor,[‡] Marek Duczmal,[†] Zbigniew Staszak,[§] and Andrzej Ozarowski[∥]

[†]Faculty of Chemistry and [§]Institute of Informatics, Wrocław University of Technology, Wybrzeże Wyspiańskiego 27, 50-370 Wrocław, Poland

[‡]Institute of Low Temperature and Structure Research, Polish Academy of Sciences, Okólna 2, 50-422 Wrocław, Poland

[∥]National High Magnetic Field Laboratory, Florida State University, 1800 East Paul Dirac Drive, Tallahassee, Florida 32310, United States

Supporting Information

ABSTRACT: The complex 2{[Ni(L-Tyr)$_2$(bpy)]}·3H$_2$O·CH$_3$OH [**1**, where L-Tyr = L-tyrosine; bpy = 2,2′-bipyridine (2,2′-bpy)] was obtained in crystalline form and characterized by X-ray and spectroscopic (FT-IR, NIR−vis−UV, and HFEPR) and magnetic methods. The complex crystallized in the hexagonal system with $a = b = 12.8116(18)$ Å, $c = 30.035(6)$ Å, and space group $P3_221$. The six-coordination sphere around the Ni^{2+} ion is formed by two N and two O L-tyrosinato atoms and completed by two N atoms of the 2,2′-bpy molecule. Neighboring [Ni(L-Tyr)$_2$(bpy)] units are joined via weak hydrogen bonds, which create a helical polymeric chain. The coordinated atoms form a strongly distorted *cis*-$NiN_2N_2'O_2$ octahedral chromophore. The solid-state electronic spectrum of complex **1** was analyzed assuming D_{2h} symmetry, and the observed bands were assigned to $^3B_{1g} \rightarrow {}^3A_g$, $^3B_{1g} \rightarrow {}^3B_{3g}$, $^3B_{1g} \rightarrow {}^3B_{2g}$, $^3B_{1g} \rightarrow {}^3B_{3g}$, $^3B_{1g} \rightarrow {}^3B_{1g}$, and $^3B_{1g} \rightarrow {}^3B_{2g}$ transitions for the I and II d−d bands, respectively. The crystal-field parameters found for D_{2h} symmetry are $Dq = 1066$ cm^{-1}, $Ds = 617$ cm^{-1}, $Dt = -93$ cm^{-1}, $B_{22} = 7000$ cm^{-1}, and Racah $B = 812$ cm^{-1}. Magnetic studies revealed the occurrence of hydrogen-bonded metal pairs. The spin Hamiltonian parameters $D = -3.262$ cm^{-1} and $E = -0.1094$ cm^{-1}, determined from high-field, high-frequency electron paramagnetic resonance spectra, together with a weak antiferromagnetic exchange parameter $J = -0.477$ cm^{-1}, allowed us to reproduce the powder magnetic susceptibility and field-dependent magnetization of the complex. The biological activity of **1** has been tested by using the *Fusarium solani*, *Penicillium verrucosum*, and *Aspergillus flavus* fungi strains and *Escherichia coli*, *Pseudomonas fluorescens*, *Serratia marcescens*, and *Bacillus subtilis* bacterial strains.

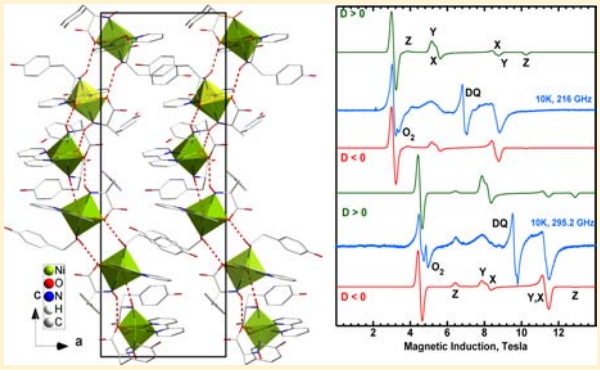

INTRODUCTION

The 2-amino-3-(4-hydroxyphenyl)propanoic acid called L-tyrosine (L-Tyr) is an essential amino acid because of its crucial importance in the synthesis of thyroxine, a thyroid hormone that is one of the most important hormones that control metabolism.[1] Also, the work of neurotransmitters such as dopamine, epinephrine, and norepinephrine, which influence emotional states, is dependent on the presence of L-Tyr. L-Tyr helps to regulate their levels in the brain and is associated with mood dysfunctions, like depression, or even with Parkinson's disease.

L-Tyr is not required in the diet because the body synthesizes it from phenylalanine. However, a deficiency of the hepatic enzyme phenylalanine hydroxylase causes a deficiency of phenylalanine, resulting in the impossibility of L-Tyr synthesis. One should keep in mind that the diet of a person suffering from phenylketonuria should be enriched by L-Tyr.[2]

L-Tyr is, in combination with alkaloids such as ephedrine, synephrine, and coffeine, an active ingredient of thermogenic drugs, which are the most effective and controversial substances used for weight loss.[3] The role of L-Tyr is optimization of noradrenaline production and the thermogenesis process.

Because of its good coordination properties, L-Tyr and its derivatives can bind various metal ions, forming complexes in solution as well as in the solid state.[4−38] Several combinations of coordination modes via amino N and carboxylate O atoms allowed the formation of typical monomers but also dimers[15,21,42b] polymers,[18,20,22,32] and a tetramer[38] that exhibit interesting spectroscopic, thermodynamic, and magnetic properties. Additionally, OH groups of phenolate rings are involved in hydrogen bonding and form $\pi-\pi$ stacking as well as

Received: November 14, 2012
Published: March 27, 2013

   dx.doi.org/10.1021/ic3024919 | *Inorg. Chem.* 2013, 52, 4360−4371

one- (1D) and three-dimensional (3D) supramolecular networks.[7] The monomers show a 1D structure and weak antiferromagnetic interaction,[32a] while the dimers exhibit strong antiferromagnetic exchange coupling.[42b]

It is well-known that interaction between protein and nucleic acid is essential for the expression and regulation of genetic information in cells. Thus, the nonelectrostatic interactions of L-Tyr with DNA and ATP have been also recognized.[39−41] This amino acid forms insoluble complexes with n-DNA and d-DNA nucleotides, whose formation is strongly dependent on the solution pH and conformation of L-Tyr.[39] Studies of this interaction were performed on L-tyrosinatocopper(II) and -platinum(II) complexes containing coligands such as 2,2′-bipyridine (2,2′-bpy), 1,10-phenanthroline (1,10-phen), or dipyrido[3,2-*a*:2′,3′-*c*]phenazine.[42−47] Especially, wide interest has been related to the DNA binding properties such as viscosity to the DNA, oxidative DNA cleavage, and anticancer activity of copper(II) ion compounds.[42,46] It seems certain that the affinity of these complexes to DNA is raised by some secondary ligands, i.e., the presence of 1,10-phen brings about the anticancer activity of the [Cu(L-Tyr)(1,10-phen)]ClO_4 complex, which is comparable to that of the drug *cis*-platin.[4] To the best of our knowledge, the L-tyrosinatonickel(II) 2,2′-bipyridino or 1,10′-phenatrolino analogues have not been synthesized.

L-Tyr is an L-phenylalanine (L-Phe) derivative, and both contain phenolate rings. It is noteworthy that L-Phe or its derivatives form decidedly fewer nickel(II) complexes than L-Tyr.[48] Likewise, amino acids containing the heterocyclic ring, i.e., proline, histidine,[49] and tryptophan[50] and their derivatives, do not form too many nickel(II) complexes. A few more examples exist in which the amino acids with the aliphatic side chain are involved, i.e., glycine (gly),[51] alanine,[52] valine,[52d,53] leucine,[52d,e,54] and isoleucine.[55]

Nickel(II) complexes of L-Tyr and its derivative *N*-(2-hydroxy-1-naphthalidene)-L-tyrosine exhibit a six-coordinated octahedrally distorted environment around metal ions and are mononuclear. L-Tyr entities chelate the Ni^{2+} ion via amino N and one carboxylato O atoms.[5,6,7a,b,28] The intermolecular interactions are transmitted by hydrogen bonds, which are formed by the phenol groups of L-Tyr and the lattice water. The hydroxyl groups are engaged in an O···O interaction network in a zigzag pattern.[7b] These interactions cause the formation of a mixed layer of hydrogen-bonding and hydrophobic interaction, named the amphiphilic layer. Such a type of packing is frequently useful as a structural model of nickel(II)-containing superoxide dismutase. Also, an interesting aspect is the comparison of the biological activity of the structurally uncharacterized L-tyrosinatonickel(II) complex and the antifungal drug Fluconazole. This drug does not inhibit the growth of animal fungi such as *Aspergillus fumigates* and *Candida albicans* as well as plant fungi such as *Penicillium sp*. In contrast, the nickel(II) L-tyrosine complex efficiently inhibited the growth of those fungi even for two applied doses of 250 and 500 μg $disk^{-1}$.[30] The physicochemical and biological properties of complexes containing both Ni^{2+} ions and the L-Tyr entity have been relatively rarely characterized.[5−7,28,30] Structural studies on such nickel(II) complexes obtained in crystalline form are particularly rare. The structural properties have been successfully related to the biological activity for only two L-tyrosinatonickel(II) complexes[28] deposited in the Cambridge Structural Database (CSD).[56]

As a continuation of our previous research, we present here structural, Fourier transform infrared (FT-IR), near-infrared (NIR)−vis−UV and high-magnetic-field electron paramagnetic resonance (HFEPR) studies on the interaction of the L-tyrosinato ligand with metal ions, combined with magnetic characterization of the complex 2{[Ni(L-Tyr)$_2$(bpy)]}·3H_2O·CH_3OH (**1**) and completed by investigation of its antifungal and antibacterial activity. The title complex **1** is the second case of the [Ni(amino acid)$_{1-2}$(bpy)] structure. Among the 20 α-amino acids, only gly forms complexes containing the Ni^{2+} ion and either 2,2′-bpy or 1,10-phen, [Ni(gly)$_2$(bpy)]·3H_2O and [Ni(gly)$_2$(phen)]·3H_2O, which are isostructural.[57] No analogous L-tyrosinatonickel(II) complexes containing 2,2′-bpy or 1,10-phen have been reported. Opposite to the copper(II) complexes of the general formula [Cu(amino acid)$_{1-2}$(bpy or phen)],[58−65] there has been so far only one known crystal structure of (amino acid)nickel(II) complexes involving 2,2′-bpy as a secondary ligand.[57]

EXPERIMENTAL SECTION

Materials. All chemicals were of reagent-grade and were used as received. Anhydrous $NiCl_2$ was purchased from Fluka. L-Tyrosine disodium salt hydrate and 2,2′-bipyridine (2,2′-bpy) were obtained from Sigma-Aldrich. Dimethyl sulfoxide (DMSO) used for recording the electronic spectra and in biological studies was obtained from Fluka.

Synthesis of the Complex 2{[Ni(L-Tyr)$_2$(bpy)]}·3H_2O·CH_3OH (1). A total of 5 mL of a 0.1 M aqueous solution of $NiCl_2$ was slowly mixed with 5 mL of a 0.1 M methanolic solution of 2,2′-bpy. After 15 min, to the red clear mixture formed above was added dropwise 10 or 15 mL of a 0.1 M aqueous solution of disodium L-tyrosinate. The obtained dark-gray clear mixture was slowly evaporated at room temperature, and deep-gray crystals of complex **1** were obtained within 2 days. The crystals were filtered and washed with water, and one of them was X-ray characterized. Anal. Calcd for $C_{57}H_{66}N_8O_{16}Ni_2$ (MW 1236.56): C, 55.37; H, 5.38; N, 9.06; Ni, 9.49. Found: C, 54.65; H, 5.53; N, 8.71; Ni, 9.15. Although the elemental analysis results are somewhat unsatisfactory, the formula of compound **1** is well supported by the X-ray structure (see Tables 1−3).

Crystallography. The crystal structure of **1** was determined by single-crystal X-ray diffraction analysis. The diffraction intensities were collected on a KUMA KM4-CCD diffractometer operating in κ geometry and equipped with a two-dimensional CCD detector. Mo Kα radiation (0.71073Å) was used. Data were collected in ω-scan mode with $\Delta\omega$ = 1.0 ° using the *CrysAlis CCD* program. *CrysAlis RED* software, version 1.170.32 (Oxford Diffraction),[66] was used for data processing. Empirical absorption correction was applied using spherical harmonics, as implemented in the *SCALE3 ABSPACK* scaling algorithm. The structure was solved by direct methods and refined by the full-matrix least-squares method against F^2 using the *SHELX-97* program package.[67] Anisotropic displacement parameters were applied for all non-H atoms. The H atoms from the organic part, which were not involved in hydrogen-bonding interactions, were generated geometrically (C−H 0.96 Å) and treated as riding atoms. The $U_{iso}(H)$ values were constrained to be xU_{eq}(carrier atom), where x = 1.2. Two disordered solvent molecules (CH_3OH and H_2O) with an occupancy factor of 50% and an ordered water molecule were located from the difference Fourier maps. The H atoms of the disordered molecules were not identified, whereas those bonded to ordered water O atoms were located based on the difference Fourier maps and the geometry of the surrounding water (taking into account the donor and acceptor abilities of the water molecule). The positions of the H atoms of the OH groups and of water molecules involved in the hydrogen bonds were refined with distance restraints applied to the donor atom (O−H 0.99 Å; σ = 0.01), whereas those of the NH_2 groups were refined without restraints.

dx.doi.org/10.1021/ic3024919 | *Inorg. Chem.* 2013, 52, 4360−4371

Table 1. Crystal Data, Experimental Details, and Structure Refinement Results for Complex 1

chemical formula	$C_{57}H_{66}N_8O_{16}Ni_2$
M_w	1236.56
cryst syst	hexagonal
space group	$P3_22_1$
temperature/K	295
a/Å	12.8116(18)
c/Å	30.035(6)
V/Å^3	4269.4(12)
Z	3
μ/mm^{-1}	0.74
cryst size/mm	0.2 × 0.18 × 0.15
T_{min}, T_{max}	0.725, 1.000
no. of measd, indep, and obsd reflns [$I > 2\sigma(I)$]	44378, 5402, 3653
R_{int}	0.099
$R[F^2 > 2\sigma(F^2)]$	0.048
$R_w(F^2)$	0.092
S	1.08
no. of reflns	5402
no. of param	406
no. of restraints	7
H-atom treatment	H atoms treated by a mixture of independent and constrained refinement
$\Delta\rho_{max}$, $\Delta\rho_{min}$/e Å^{-3}	0.29, −0.18
absolute structure	(68)
Flack parameter[68]	−0.004 (16)

Table 2. Selected Bonds (Å) Distances and Angles (deg) in Complex 1[a]

Distances			
Ni1−O2	2.048(3)	Ni1−N1	2.086(3)
Ni1−N2	2.069(3)	Ni1−N4	2.082(4)
Ni1−O4	2.055(3)	Ni1−N3	2.095(4)
Angles			
O2−Ni1−N2	91.43(12)	O4−Ni1−N4	94.50(14)
O2−Ni1−O4	96.14(12)	N1−Ni1−N4	96.02(13)
N2−Ni1−O4	80.95(13)	O2−Ni1−N3	91.55(13)
O2−Ni1−N1	80.38(12)	N2−Ni1−N3	97.81(13)
N2−Ni1−N1	167.79(13)	O4−Ni1−N3	172.24(13)
O4−Ni1−N1	90.87(13)	N1−Ni1−N3	91.49(14)
O2−Ni1−N4	168.81(14)	N4−Ni1−N3	77.90(15)
N2−Ni1−N4	93.66(13)		

[a]Symmetry transformation used to generate equivalent atoms: (i) $x - y, -y, -z + {}^1/_3$.

Table 3. Hydrogen-Bonding Interactions in the Crystal Structure of 1[a]

D−H···A	d(D−H)/Å	d(H···A)/Å	d(D···A)/Å	∠DHA/deg
N1−H1A···O4^{i}	0.82(4)	2.72(4)	3.394(5)	141(4)
N2−H2A···O2^{ii}	0.93(4)	2.30(4)	3.080(4)	140(3)
O3−H3···O1^{iii}	0.99(1)	1.73(4)	2.635(5)	149(7)
O6−H61···OW1^{iv}	0.99(1)	1.79(5)	2.693(5)	151(8)
OW1−H11···O5	0.99(1)	1.70(2)	2.688(5)	174(4)
OW1−H12···O^{v}	1.00(1)	1.89(3)	2.861(9)	163(8)

[a]Symmetry transformations used to generate the equivalent atoms: (i) $x - y, -y, -z + {}^1/_3$; (ii) $y, x, -z$; (iii) $x - y + 1, -y + 1, -z + {}^1/_3$; (iv) $y + 1, x, -z$; (v) $y, x - 1, -z$.

Physicochemical and Spectroscopic Studies. Elemental analysis for Ni^{2+} ions was performed by the ICP-AES method and that for CHN using the Kumpan method.

The vibrational FT-IR spectra were taken for complex **1** and both ligands (L-tyrosine sodium salt and 2,2′-bpy). IR spectra over the range 4000−50 cm^{-1} were recorded in KBr pellets (0.5 wt % mass) or Nujol mulls using a Perkin-Elmer FTIR-2000 spectrophotometer with resolutions of 4 and 2 cm^{-1}, respectively.

The NIR−vis−UV electronic spectra (diffuse, single-crystal absorbance, and in DMSO solvent) were obtained on a Cary 500 Scan spectrophotometer over the range 5000−50000 cm^{-1} with a resolution (measure step) of 10 cm^{-1} at 293 K. Solid-state reflectance spectra were measured for complex **1**, L-tyrosine disodium salt, and 2,2′-bpy with identical parameters as a baseline of the white reference sample. Absorbance spectra were recorded for complex **1** and ligands in a DMSO solution with concentrations of 5.23 × 10^{-2} M (**1**), 1.78 × 10^{-3} M (L-tyrosine salt), and 1.00 × 10^{-3} M (2,2′-bpy). All electronic spectra of complex **1** were enhanced by using the variable digital method.[69−71] This method, described by Bierman and Ziegler,[69] was used for analytical purposes and later adopted for analysis of the electronic and vibrational spectra.[70,71] The method uses a single convolution of the spectral points measured at equal steps with a filter function $a(n)$:

$$T(k) = \sum_{n=-N}^{N} a(n)\, f(k-n)$$

where $a(n) = (2\alpha + 1)/(2N + 1) - 2\alpha|n|/N(N + 1)$. N is the actual number of the sum component ($-N < n < N$), $T(k)$ is the filtered value in the kth measured point, f is the unfiltered spectrum, N is the filter width, and α is a real number determining the degree of resolution enhancement. By varying α and N, one can achieve different degrees of noise reduction, an increase in the height, and a decrease in the width of the component bands.

In order to obtain the approximate band positions for spectra of complex **1**, we used step = 50 cm^{-1}, α = 200, and N = 15.

Additionally, the single-crystal absorbance spectrum was deconvoluted into Gaussian components using a modification of the nonlinear least-squares algorithm,[72,73] which allowed us to obtain the exact band positions and their intensities and half-widths.

High-Frequency EPR (HFEPR) and Magnetic Measurements. High-field HFEPR spectra at temperatures ranging from ca. 6 to 290 K were recorded on a home-built spectrometer at the EMR facility of the NHMFL.[74] The instrument is a transmission-type device in which microwaves are propagated in cylindrical lightpipes. The microwaves were generated by a phase-locked Virginia Diodes source, generating a frequency of 13 ± 1 GHz and producing its harmonics, of which the 2nd, 4th, 6th, 8th, 16th, 24th, and 32nd were available. A superconducting magnet (Oxford Instruments) capable of reaching a field of 17 T was employed. The sample (50 mg) was very carefully ground, yet the effects of the microcrystals were still observed as false noise seen within the spectrum but not outside (Figure 7). The powder sample was not constrained and showed no magnetic torquing at high magnetic fields.

The magnetic susceptibility of complex **1** in the temperature range from 1.7 to 300 K in a field of 500 mT and magnetization up to 5 T were measured with a Quantum Design SQUID magnetometer. The powder samples were pressed into pellets to avoid magnetic torquing. The diamagnetic correction (−342 × 10^{-6} emu mol^{-1}) was calculated using Pascal's constants.

Microbiological Investigation. The filter paper disk method was used for the in vitro study of antibacterial effects against Gram-negative *Escherichia coli*, *Pseudomonas fluorescens*, and *Serratia marcescens* and Gram-positive *Bacillus subtilis*. Additionally, the antifungal properties of our compounds were tested on plant fungi *Fusarium solani* and *Penicillium verrucosum* and animal fungus *Aspergillus flavus*. This method is based on diffusion of a compound (metal salt, ligands, or metal complexes) solution from a filter paper disk through the solidified culture media on a Petri dish and measurement of the zone around the filter paper in which the growth

dx.doi.org/10.1021/ic3024919 | Inorg. Chem. 2013, 52, 4360−4371

of microorganisms is entirely inhibited.[29] The strains of bacteria and fungi were stored on Nutrient Agar Medium and Sabourand Agar Medium with chloramphenicol, respectively, at 4 °C.

Before the tests, the isolates of bacteria and fungi were seeded in tubes with Nutrient Broth and liquid Sabourand Medium with chloramphenicol, respectively. The solutions were incubated in a thermostat bath at 25 °C for 24 h. The seeded inoculum of microorganisms (1 mL) was homogenized in the tubes with melted media (9 mL) at 45 °C. Subsequently, the homogeneous suspensions were poured into Petri dishes and cooled. The disks of filter paper (4 mm diameter) were placed on top of the solidified media and were saturated with solutions of each complex (2×10^{-5} L). The disks containing only DMSO were used as the control. The plates were incubated at 25 °C for 24 h. The inhibitory activity was measured as the diameter (in millimeters) of the observed inhibition zones (see the Supporting Information). The tests were repeated to confirm the findings, and the average readings were taken. An inhibition zone diameter over 3 mm indicates that a tested compound is active against the bacteria and fungi under investigation. The concentration of each solution was 1.0×10^{-3} M, and commercially available DMSO was used to dissolve the samples. All investigated compounds ($NiCl_2$, L-tyrosine disodium salt, 2,2′-bpy, and **1**) are well soluble in DMSO. The values of the inhibition zone were carefully determined with a margin error of ±1 mm. All biological tests were performed twice.

RESULTS AND DISCUSSION

Crystal Structure of 1. The details of data collection and reduction are given in Table 1. Table 2 presents the refined bond lengths and angles, respectively. The crystal structure of **1** is isomorphic to the $[Zn(L\text{-}Tyr)_2(bpy)]_2{\cdot}3H_2O{\cdot}CH_3OH$ structure reported by us earlier.[75] The asymmetric unit contains one independent $[Ni(L\text{-}Tyr)_2(bpy)]_2$ complex and molecules of solvents (water and methanol). The coordination sphere can be described as a distorted octahedron with C_1 symmetry. The atoms coordinated to Ni^{2+} form a six-coordinated *cis*-$N_2N_2'O_2$ chromophore (Figure 1). The L-Tyr anions are bonded to the

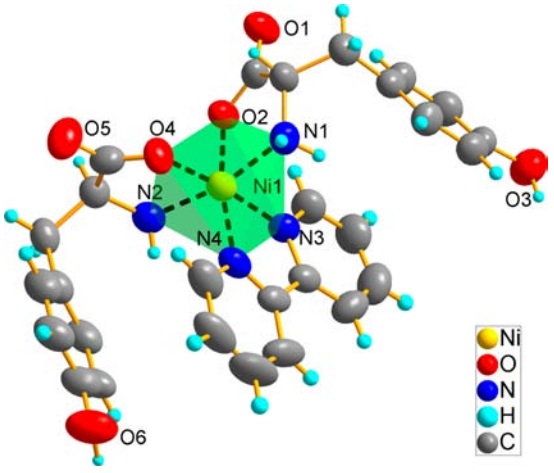

Figure 1. Distorted octahedral coordination around the Ni^{2+} center in the structure of **1**.

Ni^{2+} ions via amino N and one carboxylate O atoms. Such chelating coordination is most frequently observed for L-Tyr.[4−28,42−45,75] In the coordination sphere, the bond angles are much more distorted than the bond lengths, although deformation is weaker compared to the Zn^{2+} ion environment in the $[Zn(L\text{-}Tyr)_2(bpy)]_2{\cdot}3H_2O{\cdot}CH_3OH$ analogue. The Ni−O distances [Ni−O2 2.048(3) Å and Ni−O4 2.055(3) Å] are only slightly shorter than the Ni−N bonds [Ni1−$N2_{L\text{-}Tyr}$ 2.069(3) Å, Ni1−$N1_{L\text{-}Tyr}$ 2.086(3) Å, Ni1−N4 2.082(4) Å, and Ni1−N3 2.095(3) Å]. The Ni−$N_{L\text{-}Tyr}$ and Ni−O lengths are very close to those previously reported for other L-tyrosinatonickel(II) complexes.[5,28] However, all six bond lengths Ni−O and Ni−N in **1** are definitely longer than the Zn−O and Zn−N distances in a zinc(II) analogue.[75]

The axial positions of the octahedron are occupied by the amino N atoms. The arrangement N1−Ni−N2 is strongly nonlinear with an angle of 167.8(14)°. The distorted equatorial square plane is formed by two 2,2′-bpy N and two carboxylate O atoms. The most pronounced angular deformation concerns the N4−Ni1−N3 and O2−Ni−O4 angles, which are 77.9(2) and 96.1(1)°, respectively. The difference in the bite angles of 2,2′-bpy and L-Tyr is also less pronounced compared to that of the Zn^{2+} ion environment.[75] The N3−Ni1−N4 bite angle in the 2,2′-bpy molecule is 78.0(2)°, whereas the N2−Ni1−O4 and O2−Ni1−N1 bite angles of two L-Tyr ligands are 81.0(1) and 80.4(1)°, respectively. In 2,2′-bpy, the pyridine rings are twisted along the C19−C24 bond with a C20−C19−C24−N4 torsion angle of 172.7(7)°. As a consequence of strong intermolecular hydrogen bonding, the conformations of both amino acids (A and B) differ remarkably. The carboxylate group in L-Tyr(B) is almost coplanar to the C−N bond with a N2−C11−C10−O4 torsion angle of 4.0(6)°, whereas the corresponding angle in L-Tyr(A) is 18.7(6)°. As is found for other L-tyrosinato metal-ion complexes, the aromatic residues are characteristically bent in the same direction [C2−C3−C4 114.2(4)° and C11−C12−C13 115.3(4)°]. These angles are also slightly larger than those found in a zinc(II) complex analogue.[75]

The supramolecular structure of complex **1** is organized by numerous intermolecular O−H···O and N−H···O hydrogen bonds (Table 3). The complex is a monomer but neighboring $[Ni(L\text{-}Tyr)_2(bpy)]$ units are joined via N2−H2A···$O2^{ii}$ and N1−H1A···$O4^{i}$ hydrogen bonds between the coordinated carboxylate O atom and amine group, forming a helical polymeric chain based on hydrogen-bonding systems propagating along the [0 0 1] direction (Figure 2). There are two intrachain distances between neighboring Ni^{2+} ions of 5.933(1) and 5.868(1) Å (Figure 3). The pitch of the helix is 30.035(6) Å, whereas the separation distance between the chains is 12.8116(2) Å. Besides the N−H···O intrachain bonding, there exists another hydrogen-bonding interaction between two L-Tyr(A) from neighboring chains. The uncoordinated O atom from the carboxylate group interacts via the O3−H3···$O1^{iii}$ bond with the hydroxyl O atom, with an angle of 149(7)° and a distance of 2.635(5) Å, which is the closest intermolecular contact between the non-H atoms.

The presence of disordered solvents that simultaneously act as hydrogen donors and acceptors introduces additional interactions that hold the complex 3D hydrogen-bonding network. Strong hydrogen bonds are formed between the O atoms of amino acids and solvent water molecules as well as between solvents (Table 3). The uncoordinated carboxylate O5 atom is engaged in a relatively strong hydrogen bond, OW1−H11···O5 [2.688(5) Å], with atoms of the water molecule. Additionally, atoms of this water molecule create two hydrogen bonds, O6−H61···$OW1^{iv}$ and OW1−H12···O^{v}, together with the O6 atom of the L-Tyr hydroxyl group and the O atom of methanol. The role and geometry of these interactions has been described in detail for $[Zn(L\text{-}Tyr)_2(bpy)]_2{\cdot}3H_2O{\cdot}CH_3OH$.[75] Because the character and strength of the bonding are very similar in both crystals, we refer to the comprehensive discussion in ref 75.

dx.doi.org/10.1021/ic3024919 | Inorg. Chem. 2013, 52, 4360−4371

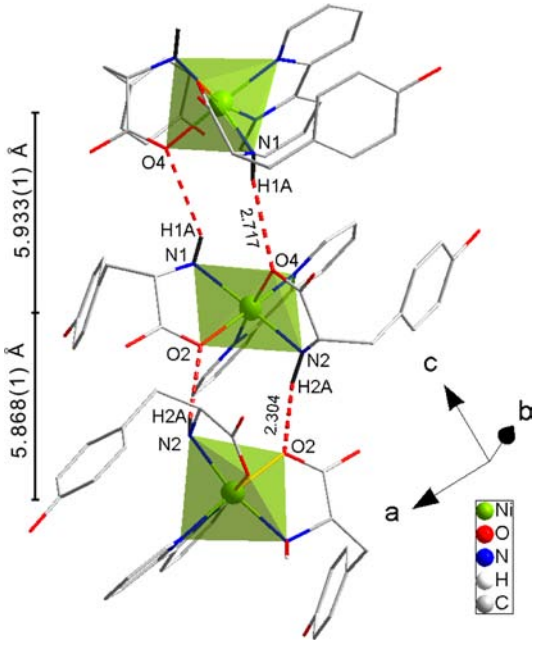

Figure 2. Hydrogen bonds between [Ni(L-Tyr)$_2$(bpy)] centers forming a polymeric 1D structure in **1**. H atoms not involved in bonding are omitted for clarity. The distances between Ni centers are marked.

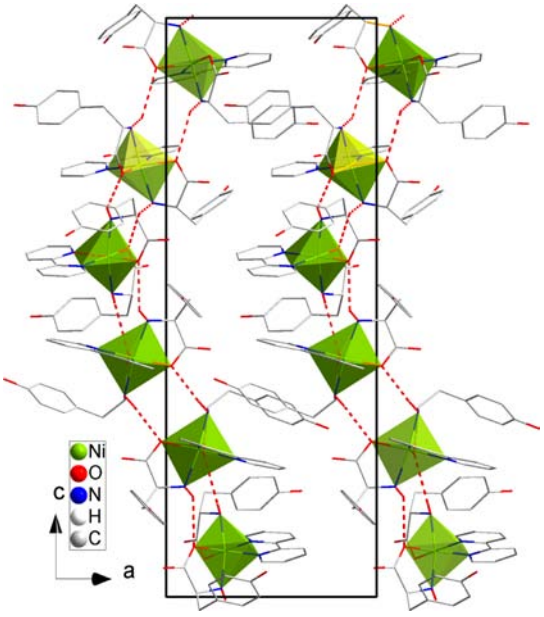

Figure 3. Helical arrangement of the [Ni(L-Tyr)$_2$(bpy)] units through N2−H2A···O2^{ii} and N1−H1A···O4^{i} interactions in complex **1**. H atoms as well as solvents are not shown for clarity.

Vibrational Spectra. The FT-IR spectra of nickel(II) complex **1** are almost identical with those of the isomorphic zinc(II) analogue.[75] In the FT-IR spectrum of **1**, the intense bands assigned to the OH, NH_2, and CH stretching vibrations of both ligands and solvent molecules are located at the highest frequencies of ca. 3500−2500 cm^{-1}. They are slightly red-shifted (ca. 300 cm^{-1}) in comparison with free L-Tyr.

In the region 1600−500 cm^{-1}, the most intense band could be distinguished at ca. 1580 cm^{-1}. This broad band consists of three overlapped components with well-seen maxima at 1598 (vs), 1581 (vs), and 1563 (vs) cm^{-1}. All bands of this region in both spectra are only 1−2 cm^{-1} blue- or red-shifted compared to spectra of the zinc(II) analogue.[75] Those bands have been correlated with asymmetric stretching vibrations of the COO^- group and sciss(NH_2) of amino acid molecules and ν(C−C) of both ligand rings. The strong band found in the FT-IR spectrum of **1** at 1514 cm^{-1} is characteristic for all L-tyrosinatocopper(II), -zinc(II), and nickel(II) metal-ion complexes studied previously[18,28,75] and originates from the ring ν(C−C) vibration, which appears at 1500 cm^{-1} in the IR spectrum of the L-tyrosine salt.

The coordination of both N_{bpy} and $N_{L\text{-}Tyr}$ and O atoms to Ni, seen in the X-ray structure, is in agreement with the bands observed below 500 cm^{-1}. The Ni−N_{bpy} stretching vibration results in a medium-intensity band at 227 cm^{-1}, whereas the strong band with a maximum at 414 cm^{-1} comes from Ni−$N_{L\text{-}Tyr}$.

NIR−Vis−UV Electronic Spectroscopy. *Solid-State Spectra at 298 K (Reflectance and Single Crystal at 298 K).* Reports of electronic spectra of L-tyrosinatonickel(II) complexes together with their crystal structure characterization are relatively scarce, [28] as are studies of nickel(II) complexes with L/D-Phe [48] or amino acids containing the heterocyclic rings.[49,50] As mentioned in the Introduction, only one complex consisting of Ni^{2+} ions, 2,2′-bpy, and amino acid entities, [Ni(gly)$_2$(bpy)]·3H$_2$O, has been structurally characterized along with its 1,10-phen analogue, [Ni(gly)$_2$(phen)]·3H$_2$O.[57] It is difficult to find electronic spectroscopy together with crystal structure characterization of amino acid nickel(II) complexes even if they involved heterocyclic amines of well-known coordination properties like bpy or phen.

In complex **1**, two coordinated L-tyrosinato N and two O atoms as well as two N atoms of 2,2′-bpy form the *cis*-$NiN_2N_2'O_2$ chromophore of pseudooctahedral geometry around the Ni^{2+} ion.

In the 7000−30000 cm^{-1} region, the spectrum of **1** shows two clearly marked bands centered at 10470 and 17350 cm^{-1} (Figure 4), which correspond to the I and II d−d transitions. The third band is observed only as a shoulder at ca. 25300 cm^{-1} because its high-energy part overlaps with the charge-transfer (CT) transitions. This curve is a combination of spin-forbidden and components of the III spin-allowed d−d transitions.

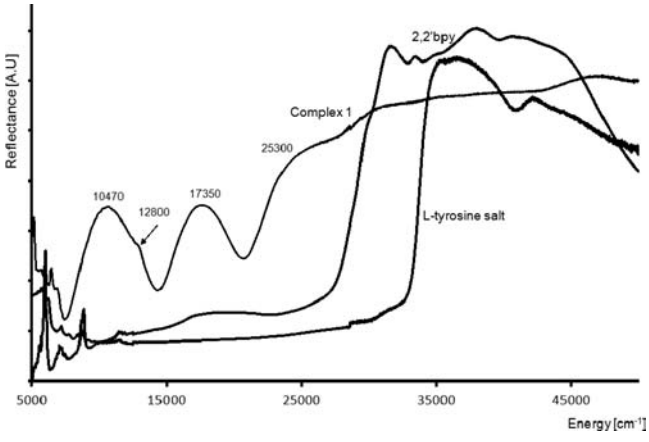

Figure 4. Diffuse solid-state reflectance spectra at 298 K and in the spectral range 5000−50000 cm^{-1} of a powder sample of **1**, free L-tyrosine salt, and 2,2′-bpy.

dx.doi.org/10.1021/ic3024919 | Inorg. Chem. 2013, 52, 4360−4371

The spectrum of **1** is comparable to the earlier characterized spectrum of the $[Ni(Im)_2(L\text{-}Tyr)_2]\cdot 4H_2O$ complex, which also contains a *cis*-$NiN_2N_2'O_2$ chromophore.[28] In **1**, the I, II, and III d−d bands exhibit red shifts of ca. 200, 50, and 2500 cm^{-1}, respectively. There are three different metal−ligand distances in the distorted octahedron of the $[Ni(Im)_2(L\text{-}Tyr)_2]$ complex [Ni−O 2.0894(14) Å, Ni−$N_{L\text{-}Tyr}$ 2.0905(16) Å, and Ni−N_{im} 2.0703(16) Å], and its reflectance and single-crystal spectra were successfully interpreted in D_{4h} symmetry.[28] The Ni−O2, −O4, −N1, −N2, −N3, and −N4 distances in the [Ni(L-Tyr)$_2$(bpy)] unit (**1**; Table 2) are all different; thus, the symmetry around the six-coordinated Ni^{2+} center is only C_1. The noticeable asymmetry of the d−d bands indicates that those bands are probably split under crystal-field symmetry lower than O_h.[76−80] This spectrum was thus filtered for the purpose of obtaining the refined band splitting and energies of its components. The filtering process revealed that the first d−d band is composed of three maxima at 9460, 10650, and 11210 cm^{-1} (Figure 5 and Table 4). The shoulder at 12800 cm^{-1} seems to be unsplit. The second d−d band includes also three components centered at 16060, 17100, and 18600 cm^{-1}. The broad band at ca. 25300 cm^{-1} consists of four components at 21800, 23010, 24450, and 25720 cm^{-1}.

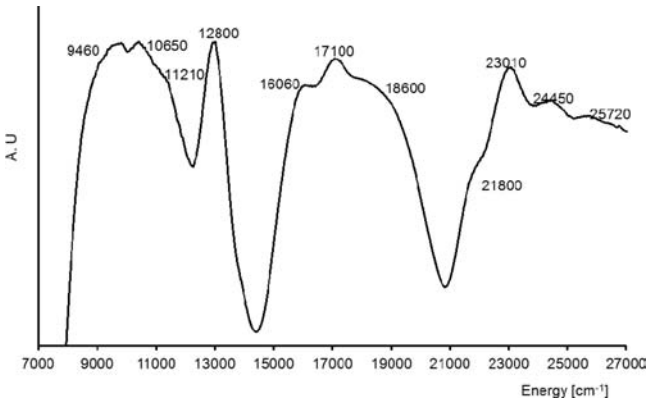

Figure 5. Effect of filtering of the solid-state spectrum of **1** in the range 7000−27000 cm^{-1} (filter parameters: step = 50, α = 200, and N = 15).

The real symmetry of the Ni^{2+} ion environment is C_1, but using the D_{2h} point group gave a good agreement between the obtained and expected number of components. The replacement of the two imidazole molecules by the chelating 2,2′-bpy molecule brings about slight changes in the d−d band positions. The most important is that it creates a stronger crystal field, which causes splitting of the first and second d−d bands into three components expected for D_{2h} symmetry.[81−83]

In $D_{2h}(C_2'')$ symmetry, the $^3B_{1g}$ term is the ground state and nine spin-allowed transitions, $^3B_{1g} \rightarrow {}^3A_g$, $^3B_{1g} \rightarrow {}^3B_{2g}$, and $^3B_{1g} \rightarrow {}^3B_{3g}$ (I^{st} d−d), $^3B_{1g} \rightarrow {}^3B_{1g}$, $^3B_{1g} \rightarrow {}^3B_{2g}$, and $^3B_{1g} \rightarrow {}^3B_{3g}$ (II d−d), $^3B_{1g} \rightarrow {}^3B_{1g}$, $^3B_{1g} \rightarrow {}^3B_{2g}$, and $^3B_{1g} \rightarrow {}^3B_{3g}$ (III d−d), are possible as a result of splitting of $^3T_{2g}(^3F,O_h)$, $^3T_{1g}(^3F,O_h)$, and $^3T_{1g}(^3P,O_h)$ states in a rhombic crystal field (Table 4).[76−83] The three components of the I d−d band are centered at 9460, 10650, and 11210 cm^{-1}, respectively. The II d−d band includes three separate components obtained at 16060, 17100, and 18600 cm^{-1}. The band at 25720 cm^{-1} could probably be assigned to the first components of the III d−d band. Likewise, the crystal field of D_{2h} symmetry causes splitting of the $^1E_g(^1F)$ and $^1T_{2g}(^1D)$ levels into $A_g + B_{1g}$ and $B_{2g} + B_{3g} + A_g$ states, respectively. In the filtered spectrum, a sharp profile is clearly seen at 12800 cm^{-1} but without evidence of a splitting and it can be correlated with the combined spin- and symmetry-forbidden transition $^1E_g \rightarrow A_g + B_{1g}$. The successive bands found at 21800 and 23010 cm^{-1} arise from $^3B_{1g} \rightarrow A_g$ and $^3B_{1g} \rightarrow B_{2g} + B_{3g}$ forbidden transitions, respectively. The spin- and symmetry-forbidden $^3B_{1g} \rightarrow A_{1g}(G)$ transition is correlated with a band at 24450 cm^{-1}.

The absorbance spectrum of a single crystal of **1** resembles the reflectance spectrum (Figure 6a). The results of its filtering and Gaussian fitting are presented in Figure 6b,c. The splitting of d−d bands is noticeable, but the spin-forbidden transitions are still found as single bands (Figure 6a,b and Table 4), just like in the reflectance spectrum.

The tetragonal crystal-field parameters *Dq*, *Ds*, and *Dt* and the Racah *B* parameter were obtained using the energies of the first four spin-allowed ^3E_g, $^3B_{2g}$, $^3A_{2g}$, and ^3E_g and two lowest

Table 4. Band Assignments and Experimental and Theoretical Energies of d−d Transitions for Complex 1[a]

Symmetry			energy (cm^{-1})				
			reflectance spectrum		single crystal (293 K)		absorbance spectrum
O_h, ground state $^3A_{2g}$	D_{4h}, ground state $^3B_{1g}$	$D_{2h}(C_2'')$, ground state $^3B_{1g}$	*b*	calcd[c]	*b*	*f*	*b*, *d*, and *e*
$^3T_{2g}$ (F)	$^3B_{2g}$	^3A_g	9460	9344	9350	9547	10650 (12)
	^3E_g	$^3B_{3g}$	10650	10660	11000	11500	
		$^3B_{2g}$	11210	11034	11850	12210	
^1E_g (F)	$A_{1g} + B_{1g}$	$A_g + B_{1g}$	12800	9475 + 12612	12850	12705	12900 (6)
$^3T_{1g}$ (F)	^3E_g	$^3B_{3g}$	16060	16195	16100	16400	17650 (16)
	$^3A_{2g}$	$^3B_{1g}$	17100	17305	17000	17135	
		$^3B_{2g}$	18600	18918	18100	18385	
$^1T_{2g}$ (D)	B_{2g}	A_g	21800	21516	21500	20735	
	E_g	B_{2g}		23215			
		B_{3g}	23010	23547			
$^1A_{1g}$ (G)	A_{1g}	A_g	24450	23873			

[a]Transition energies are given in cm^{-1}. [b]Energies are taken from filtering. [c]Calculated values of energy (for the spin triplets, the mean values for three spin−orbit components are shown) were obtained for applying D_{2h} symmetry with Dq = 1066 cm^{-1}, Ds = 617 cm^{-1}, Dt = −93 cm^{-1}, B_{22} = 7000 cm^{-1}, and ζ = 570 cm^{-1}. [d]O_h symmetry. [e]Molar absorption coefficients ε in $dm^3\ mol^{-1}\ cm^{-1}$ are given in parentheses. [f]Position taken from Gaussian deconvolution.

dx.doi.org/10.1021/ic3024919 | Inorg. Chem. 2013, 52, 4360−4371

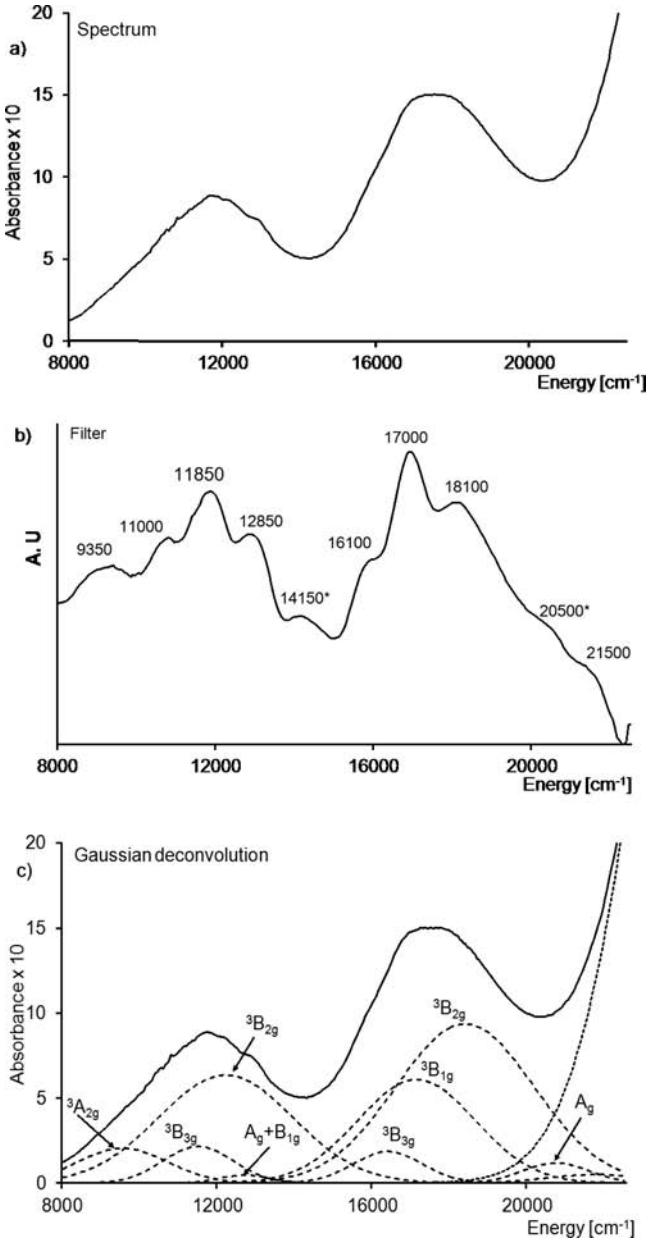

Figure 6. Single-crystal spectrum of **1**: (a) absorbance at 293 K; (b) filtered spectrum; (c) Gaussian deconvolution in D_{2h} symmetry (* effect of the noise in part b).

spin-forbidden $^1A_{1g}$ and $^1B_{1g}$ states, yielding B = 812 cm^{-1} (C = 4B), Dq = 1066 cm^{-1}, Ds = 617 cm^{-1}, and Dt = − 93 cm^{-1}. The Dq value of **1** is slightly lower than Dq (1180 cm^{-1}) found previously for the [Ni(Im)$_2$(L-Tyr)$_2$] complex.[28] This may be due to the greater ligand strength of 2,2′-bpy.

Making use of the known relationships [84] $B_{20} = -7Ds$, $B_{40} = 21(Dq - Dt)$, and $B_{44} = 21(5/14)^{1/2}Dq$, the "Wybourne" crystal-field parameters B_{kq} were obtained. The final calculation of the transition energies was performed assuming D_{2h} symmetry. After arbitrary addition of the rhombic B_{22} = 7000 cm^{-1} and the effective one-electron spin−orbit ζ = 570 cm^{-1} parameters, the Hamiltonian containing the electron−electron interactions, the spin−orbit coupling, the ligand-field potential, and the Zeeman term was diagonalized. All matrix elements were calculated using Gerloch's "master equations".[85,86] The calculated energies stand in good correlation with the experimental spectroscopic data (Table 4). Moreover, the spin−orbit interaction splits the ground spin triplet $^3B_{1g}$ by 3.25 cm^{-1}. This splitting corresponds to the $-D$ zero-field-splitting (zfs) parameter,[87] and its value is comparable with the HFEPR parameter (see infra). As a consequence, magnetization calculated with the set of spectroscopic parameters (B, C, Dq, Ds, Dt, B_{22}, and ζ) fits well the experimental data (see the Supporting Information).

Solution Absorbance Spectrum in DMSO. The solution spectrum of **1** shows two very well-developed symmetric bands with maxima at 10800 and 17700 cm^{-1}, which arise from the I and II d−d bands (Supporting Information, Figure S1). Similarly to the reflectance spectrum, the expected III band and bands assigned as spin-forbidden transitions are partly overlapped by more intense metal−ligand CT transitions and are observed only as a shoulder at 25100 cm^{-1}. The molar coefficient values are in the range 10−120 dm^3 mol^{-1} cm^{-1}, which is characteristic for d−d transitions. No splitting of the symmetric bands was obtained by using the filtering procedure, and the bands are correlated with $^3A_{2g} \rightarrow {}^3T_{2g}(^3F)$, $^3A_{2g} \rightarrow {}^3T_{1g}(^3F)$, and $^3A_{2g} \rightarrow {}^3T_{1g}(^3P)$ spin-allowed transitions in an octahedral crystal field.[28,76−79] The spin-forbidden transition $^3A_{2g} \rightarrow {}^1E_g(^1D)$ is assigned to the well-marked shoulder at 12880 cm^{-1} (Table 4 and Supporting Information, Figure S1). Calculation of the O_h crystal-field parameters taking into account the energy of the I and II d−d bands and first spin-forbidden transitions (10650, 17650, and 12900 cm^{-1}, respectively) gave Dq = 1065, B = 1121, C = 2295, and C/B = 2.05 and the theoretical energy of III d−d of 31100 cm^{-1}. The value of B is definitely higher than that of B for an isolated Ni^{2+} ion, C/B should be between 3 and 5, and the calculated band position of the $^3A_{2g} \rightarrow {}^3T_{1g}(^3P)$ transition is contrary to experimental data. Thus, the value of Dq is adequate to explain the experimental $^3A_{2g} \rightarrow {}^3T_{2g}(^3F)$ transition energy. Calculation of B from the 17650 [$^3T_{1g}(^3F)$] and 25100 cm^{-1} [$^3T_{1g}(^3P)$] transitions resulted in 672 cm^{-1}, which is acceptable. Generally, this absorbance spectrum of complex **1** dissolved in DMSO confirmed the six-coordinated environment around the Ni^{2+} ion and the *cis*-[NiN$_4$O$_2$] chromophore in solution as well as in the solid state. The fact that the complex retains its structure also in a DMSO solution is important for interpretation of the biological results.

High-Field HFEPR. The triplet-state (S = 1) EPR spectra were interpreted using the standard spin Hamiltonian (eq 1, below). The zfs parameters D and E derived from the high-frequency spectra (Figure 7) were of moderate magnitude for a Ni^{2+} ion[88,89] yet were large enough to render standard EPR inoperative.

The spin Hamiltonian parameters were found to be similar to those of a related complex, [Ni(Im)$_2$(L-Tyr)$_2$]·4H$_2$O. [28] An important advantage of the high-field HFEPR spectroscopy is the possibility of determining the sign of the zfs parameters.[28,90,91] Although the resonance fields in EPR are independent of the sign of D, the intensity pattern in a spectrum depends on it, provided that the Zeeman splitting is comparable to kT. In the present case, the high-field "Z" resonance and low-field "X" and "Y" resonances are suppressed when the temperature is lowered, while the intensity of the low-field "Z" and high-field "X" and "Y" resonances increases. This is well seen in the bottom part of Figure 7 and is diagnostic of the negative sign of D. This result is important for interpretation of our magnetic data (see below).

dx.doi.org/10.1021/ic3024919 | Inorg. Chem. 2013, 52, 4360−4371

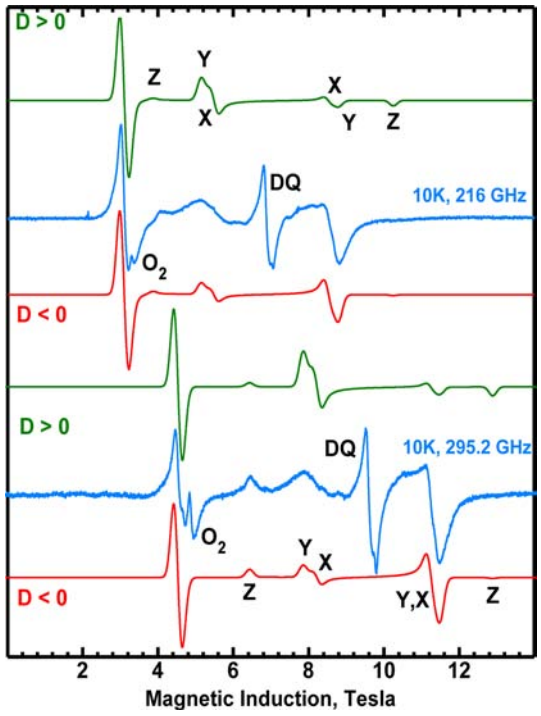

Figure 7. High-field EPR spectra measured at 10 K with the microwave frequencies 216.0 and 295.2 GHz. The simulations used spin $S = 1$, $g_x = 2.138$, $g_y = 2.156$, $g_z = 2.188$, $D = -3.262$ cm^{-1}, and $E = -0.1094$ cm^{-1}. For comparison, simulations with positive D and E are also shown. Resonances marked with O_2 are due to oxygen adsorbed on the powder sample ($S = 1$, $g_{x,y,z} = 2$, $D = 3.57$ cm^{-1}, and $E = 0$), which is typically observed in HFEPR below 30 K. DQ marks the "double quantum transition", characteristic of Ni^{2+} systems.

Magnetic Properties. The magnetic susceptibility (Figure 8) shows the Curie–Weiss behavior in the temperature range of

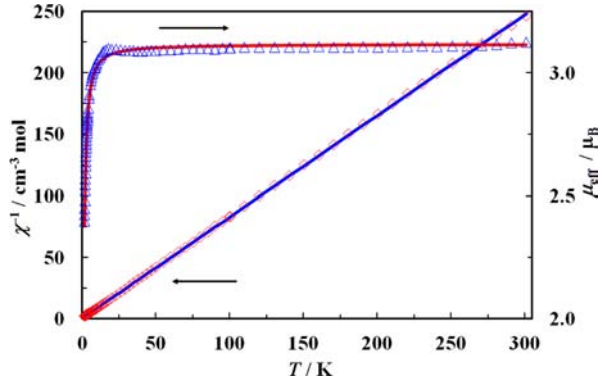

Figure 8. Plots of χ^{-1} (◇) and μ_{eff} (Δ) versus T for **1**. The solid lines correspond to the best-fit parameters.

ca. 50–250 K with a Weiss constant $\Theta = -0.7$ K and a magnetic moment of 3.11 μ_B. The moment is larger than the value of 2.83 μ_B expected for the spin-only value of an ion with $S = 1$ and $g = 2.0$ and lies within the range observed in other high-spin nickel(II) compounds. [92] The effective magnetic moment decreases slowly from 3.12 μ_B at 300 K to 3.0 μ_B at 10 K and then drops to 2.4 μ_B at 1.7 K. The decrease in the moment below 10 K could be caused by zfs and/or antiferromagnetic exchange interactions between the metal ions.

Assuming that only zfs is responsible for low-temperature effects, we have calculated the magnetization of the isolated Ni^{2+} ion by full-matrix diagonalization of the Hamiltonian:

$$\hat{H} = \mu_B \mathbf{B}\cdot\hat{\boldsymbol{g}}\cdot\hat{\boldsymbol{S}} + D\left[\hat{S}_z^2 - \frac{1}{3}S(S+1)\right] + E(\hat{S}_x^2 - \hat{S}_y^2) \quad (1)$$

Using the HFEPR parameters ($D = -3.262$ cm^{-1}, $E = -0.1094$ cm^{-1}, $g_x = 2.128$, $g_y = 2.156$, and $g_z = 2.188$), a rather poor fit of the calculated and experimental data has been obtained (see the dotted line in Figure 9). Interestingly, in a related complex,[28] a

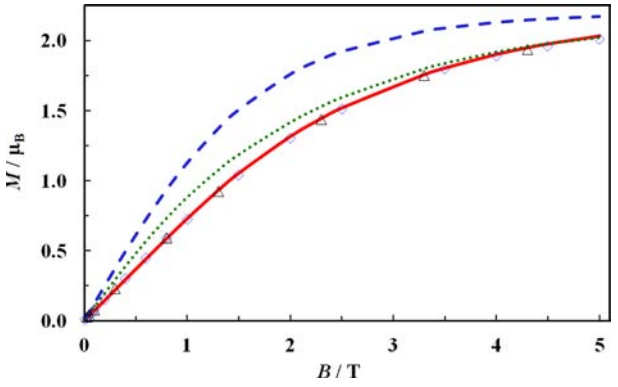

Figure 9. Magnetization as a function of magnetic induction at 1.72 K (◇, increasing field; Δ, decreasing field). The dashed line is the Brillouin function for $S = 1$ and $g = 2.204$. The dotted line is the magnetization calculated with the HFEPR parameters $D = -3.262$ cm^{-1}, $E = -0.1094$ cm^{-1}, $g_x = 2.128$, $g_y = 2.156$, and $g_z = 2.188$. The solid line uses parameters $J = -0.477$ cm^{-1}, $D = -3.262$ cm^{-1}, $E = -0.1094$ cm^{-1}, and $g_{av} = 2.204$.

perfect agreement was observed. One of the reasons for this discrepancy may be the fact that hydrogen bonds existing in **1** are able to mediate magnetic exchange coupling between metal ions.

The crystals of **1** contain alternating chains of Ni^{2+} ions. The neutral [Ni(L-Tyr)$_2$(bpy)] units are linked through the pair of hydrogen bonds involving the coordinated carboxylate O atoms and the coordinated amine group of L-Tyr (Figures 2 and 3), alternately N2–H2A···O2^{ii} bonds [d(D···A) = 3.080(4) Å, ∠(DHA) = 140(3)°, d(Ni···Ni) = 5.868(1) Å] and N1–H1A···O4^{i} bonds [d(D···A) = 3.394(5) Å, ∠(DHA) = 141(4)°, d(Ni···Ni) = 5.933(1) Å]. The first bridging motif should be a much better transmitter of magnetic superexchange. It contains not only shorter hydrogen bonds but also a more favorable atom arrangement: the angle between the neighboring NiN_3O planes engaged in hydrogen bonds is equal to 25.11°, whereas the corresponding value for the second set is 60.03°, and the reduction of this parameter would lead to a better overlap between magnetic orbitals of the metal ions. Accordingly, we have tried to fit the experimental data to a model comprised of magnetically coupled isolated dimers (N2–H2···O2 bonds; Figure 2), adding the term $-J\hat{S}_1\cdot\hat{S}_2$ to eq 1. Even though the goodness of fit was improved, the high-temperature susceptibility was still poorly simulated. Good results have been achieved when the g factor was allowed to change freely. The fitting of the temperature dependence of susceptibility (Figure 8) gave $D = -3.262$ cm^{-1}, $E = -0.1094$ cm^{-1} (HFEPR values), $g_{av} = 2.204(1)$, $J = -0.477(4)$ cm^{-1}, $R = \sum[(\chi T)_{exp} - (\chi T)_{calc}]^2/\sum[(\chi T)_{exp}]^2 = 6.8 \times 10^{-5}$ (87 points). The average g

dx.doi.org/10.1021/ic3024919 | Inorg. Chem. 2013, 52, 4360–4371

Table 5. Antibacterial and Antifungal Activities of DMSO, L-Tyrosine Salt, 2,2′-bpy, and Complex 1[a]

	mean diameter of inhibition (mm)						
	test fungi			test bacteria			
	plant fungi		animal fungus	Gram-negative			Gram-positive
	F. solani	*P. verrucosum*	*A. flavus*	*E. coli*	*P. fluorescens*	*S. marcescens*	*B. subtilis*
DMSO	0	0	0	0	0	3[b]	0
$NiCl_2·6H_2O$	2[b]	2[b]	2[b]	2	2[b]	4	0
2,2′-bpy	0	0	0	0	0	3[b]	3[b]
L-tyrosine salt	1	3	0	3[b]	0	3[b]	2[b]
$2\{[Ni(L\text{-}Tyr)_2(bpy)]\}·3H_2O·CH_3OH$ (**1**)	3[b]	3[b]	3[b]	3[b]	0	3	2[b]
$[Zn(L\text{-}Tyr)_2(bpy)]_2·3H_2O·CH_3OH$ [75]	2[b]	0	3[b]	3[b]	0	3	3[b]

[a]The diameter of the inhibition zone not including the disk diameter of 4 mm. Values are means of the average of two replications. The compound exhibits antibacterial or antifungal activities if the mean diameter of the inhibition zone iss over 3 mm. [b]Growth of microorganisms in the inhibition zone.

value is bigger by only 2% than $g_{av}^{HFEPR} = 2.157$. Such a phenomenon, when g determined from magnetic susceptibility is a little larger than EPR value, is not rare; see, for example, ref 93. Additionally, the possibility of partial loss of a non-coordinated methanol or water from complex **1** cannot be completely ruled out. Magnetic exchange and zero-field interactions strongly influence low-temperature magnetization, and the goodness of fit has been confirmed after calculation of the field-dependent magnetization. The $M(B)$ dependence measured at 1.7 K and calculated for various external fields with the same parameters as those of the susceptibility is drawn in Figure 9 as a solid line and fits the experimental data excellently. No significant improvement of the susceptibility fit was achieved after introduction of an additional coupling parameter, zJ', to account for the possible interdimer interaction between the adjacent unit through N1−H1···O4 bridges (Figure 2):[94]

$$\chi = \chi_{dimer}/[1 - (2zJ'/Ng^2b^2)\chi_{dimer}] \quad (2)$$

It led to $g_{av} = 2.202(1)$, $J = -0.53(3)$ cm^{-1}, $zJ' = 0.05(3)$ cm^{-1}, and $R = 6.5 \times 10^{-5}$. This means that the earlier assumption about a strong nonequivalence of alternating hydrogen bonds in the chain of metal ions was justified.

Intermolecular exchange coupling through hydrogen bonds is well documented. A large majority of papers deals with copper(II) dimers, and only for such types of compounds have some magnetostructural correlations been made.[95,96] Analogous nickel(II) compounds are rare.[97−103] Magnetic coupling between Ni^{2+} ions is weak ($|J|$ usually below 1 cm^{-1}) and antiferromagnetic, with one significant exception of $[Ni(L)(H_2O)_4]·2H_2O$ (H_2L = α,α′-dihydroxybibenzyl-4,4′-dicarboxylic acid),[101] with triple hydrogen bonds between face-to-face-oriented NiO_6 octahedra and relatively strong ferromagnetic interaction ($J = 5.10$ cm^{-1}). The complexes with exclusively hydrogen-bonded Ni^{2+} ions, analyzed beyond the Curie−Weiss law, are collated in ref 104.

Microbiological Studies. The biological properties of DMSO, $NiCl_2$, organic ligands, and **1** were investigated using the fungi *F. solani*, *P. verrucosum*, and *A. flavus* and bacterial strains such as *E. coli*, *P. fluorescens*, *S. marcescens*, and *B. subtilis*. The results of antibacterial and antifungal activities are presented in Table 5. The growth of bacteria and fungi is observed on the solidified culture media in a Petri dish around the filter paper disk containing the studied compound. Because pure DMSO was used as a basic solvent, its activities against all strains were primarily investigated. DMSO is the most often used solvent in such biological studies.[28−30,105] In control tests, in which DMSO only was used, the inhibition zones equal zero, which implies that this solvent has not inhibited microorganism growth. Similarly, the $NiCl_2$ salt exhibited a weak inhibition effect (Supporting Information, Figure S4). 2,2′-bpy is entirely inactive. The L-tyrosine salt impeded the growth of microorganisms a little better. Among these tested compounds, complex **1** seems to be the most active. However, the test for **1** revealed a decidedly weak effect in comparison to our earlier results obtained for $[Cu(L\text{-}Tyr)_2]_n$, $[Ni(L\text{-}Tyr)_2(H_2O)_2]·H_2O$, and $[Ni(Im)_2(L\text{-}Tyr)_2]·4H_2O$ complexes.[28] Complex **1** inhibited the growth of only one Gram-negative bacterium, *S. marcescens*. Unfortunately, growth of all other microorganisms in inhibition zones was observed. If the inhibition zone size of 3 mm is adopted as a minimum, then it must be concluded that complex **1** does not inhibit adequately microorganism growth. This behavior resembles that found for the zinc(II) complex $[Zn(L\text{-}Tyr)_2(bpy)]_2·3H_2O·CH_3OH$ (Table 5).[75] Thus, the biological results for both isomorphic complexes show that the inhibition activity is independent of the presence of Ni^{2+} or Zn^{2+} ions.

In our previous paper,[28] we demonstrated that the activity of the $[Ni(Im)_2(L\text{-}Tyr)_2]·4H_2O$ complex containing both the L-Tyr and imidazole molecules is definitely higher compared to those of complex **1** studied here and $[Ni(L\text{-}Tyr)_2(H_2O)_2]·H_2O$.[28] Upon comparison of the activities of **1** to $[Ni(L\text{-}Tyr)_2(H_2O)_2]·H_2O$ and $[Ni(Im)_2(L\text{-}Tyr)_2]·4H_2O$, it was found that the increase in the antifungal and antibacterial activities caused by the presence of a secondary ligand follows the sequence 2,2′-bpy < H_2O < imidazole. This sequence is similar to that found for the zinc(II) complexes like $[Zn(L\text{-}Tyr)_2(bpy)]_2·3H_2O·CH_3OH$, $\{[Zn(L\text{-}Tyr)_2(H_2O)]·H_2O\}_n$, and $[Zn(Im)(L\text{-}Tyr)_2]_2·5H_2O$.[75]

CONCLUSIONS

This work was focused on broad physicochemical characterization of a new L-tyrosinatonickel(II) complex, **1**, in combination with biological studies. The crystal structure of **1** is just the second case (besides $[Ni(gly)_2(bpy)]·3H_2O$) of a complex built of the $[Ni(amino\ acid)_2(bpy)]$ units.

The two L-Tyr anions chelate the Ni^{2+} ion via one of the carboxylate O and N amino atoms and together with two 2,2′-bpy N atoms form the distorted octahedral *cis*-$NiN_2N_2'O_2$ chromophore. The crystal structure of **1** is built of monomeric $[Ni(L\text{-}Tyr)_2(bpy)]$ units as well as disordered water and methanol molecules. The closest nickel−nickel distances in the

dx.doi.org/10.1021/ic3024919 | Inorg. Chem. 2013, 52, 4360−4371

crystal lattice are 5.933(1) and 5.868(1) Å. The structure is stabilized by numerous hydrogen bonds. The strong hydrogen bonds are found between water and methanol atoms and the O atoms of L-tyrosinato hydroxyl and carboxylate groups. The weak hydrogen bonds based on the amino N and carboxylate O atoms, N2−H2A···O2^{i} and N1−H1A···O4^{v}, play an important role in creating the helical polymeric chain structure. The filtering process of reflectance spectra allowed us to find three components of the first and second d−d bands (D_{2h}), which are correlated with $^3B_{1g} \rightarrow {}^3A_g$, $^3B_{1g} \rightarrow {}^3B_{3g}$, and $^3B_{1g} \rightarrow {}^3B_{2g}$ (I d−d) and $^3B_{1g} \rightarrow {}^3B_{3g}$, $^3B_{1g} \rightarrow {}^3B_{1g}$, and $^3B_{1g} \rightarrow {}^3B_{2g}$ (II d−d) transitions with energies 9460, 10650, 11210, 16060, 17100, and 18600 cm^{-1}, respectively. The theoretical energies of transitions obtained for D_{2h} symmetry gave the crystal-field parameters Dq = 1066 cm^{-1}, Racah B = 812 cm^{-1} ($C = 4B$), Ds = 617 cm^{-1}, Dt = −93 cm^{-1}, and B_{22} = 7000 cm^{-1}. Additionally, this parameter set, complemented by the effective spin−orbit parameter ζ = 570 cm^{-1}, provided a reasonable simulation of the temperature- and field-dependent magnetization. Complex **1** maintains its six-coordinated structure in a DMSO solution.

The zfs parameters derived from HFEPR experiments yielded satisfactory agreement between the measured and calculated magnetization only after a weak antiferromagnetic exchange interaction transmitted through hydrogen bonds between metal ions is taken into account. The antifungal and antibacterial activities of **1** and [Zn(L-Tyr)$_2$(bpy)]$_2$·3H$_2$O·CH$_3$OH complexes are weak and independent of the kind of metal ion. However, a comparison of those activities for **1**, [Ni(L-Tyr)$_2$(H$_2$O)$_2$]·H$_2$O, and [Ni(Im)$_2$(L-Tyr)$_2$]·4H$_2$O shows that the secondary ligand plays an important role in increasing the inhibition zone. The biological activities of three L-tyrosinatonickel(II) complexes increase in the sequence 2,2′-bpy < H$_2$O < imidazole.

■ ASSOCIATED CONTENT

Supporting Information

X-ray crystallographic data in CIF format for **1**, tables, and supplementary figures. This material is available free of charge via the Internet at http://pubs.acs.org. Crystallographic data for **1** have also been deposited with the Cambridge Crystallographic Data Centre and are available at www.ccdc.cam.ac.uk/data_request/cif under CCDC 888955.

■ AUTHOR INFORMATION

Corresponding Author

*E-mail: agnieszka.wojciechowska@pwr.wroc.pl. Phone: +48 713203666. Fax: +48 71 320 43 60.

Notes

The authors declare no competing financial interest.

■ ACKNOWLEDGMENTS

The work was financed by a statutory activity subsidy from the Polish Ministry of Science and Higher Education for the Faculty of Chemistry of Wrocław University of Technology. The high-field EPR spectra were recorded at the NHMFL, which is funded by the NSF through the Cooperative Agreement DMR-0654118, the State of Florida, and the DOE. The authors also thank Dr. A. Trusz-Zdybek for the biological tests.

■ REFERENCES

(1) Chalmers, J. R.; Dickson, G. T.; Elks, J.; Hems, B. A. *J. Chem. Soc.* **1949**, 3424−3433.
(2) Spronsen, F. J.; Rijn, M.; Bekhof, J.; Koch, R.; Smit, P. *Am. J. Clin. Nutr.* **2001**, *73*, 153−157.
(3) Hull, K. M.; Maher, T. *J. Pharmacol. Biochem. Behav.* **1992**, *43*, 1047−1052.
(4) Ramakrishna, S.; Rajendiran, V.; Palaniandavar, M.; Periasamy, V. S.; Srinag, B. S.; Krishnamurthy, H.; Akbarsha, M. A. *Inorg. Chem.* **2009**, *48*, 1309−1322.
(5) Hamalainen, R.; Lajunen, K.; Valkonen, J. *Finn. Chem. Lett.* **1977**, *4 − 5*, 108−112.
(6) (a) Hamalainen, R.; Ahlgren, M.; Turpeinen, U.; Raikas, T. *Cryst. Struct. Commun.* **1978**, *7*, 379−384. (b) Gao, Ch.; Ma, X.; Kou, Y.; Li, D.; Feng, L.; Tian, J.; Yan, S. *Acta Sci. Nat. Univ. Nankaiensis* **2009**, *42*, 103−104.
(7) (a) Pei, Y.; Wang, L. *Acta Crystallogr., Sect. E* **2006**, *62*, m1668−m1670. (b) New, S. Y.; Wu, X.; Bai, S.-Q.; Koh, L.; Hor, T. S. A.; Xue, F. *CrystEngComm* **2011**, *13*, 4228. (c) Ebel, M.; Rehder, D. *Inorg. Chem.* **2006**, *45*, 7083−7090.
(8) Kiss, T.; Gergely, A. *J. Chem. Soc., Dalton Trans.* **1984**, 1951−1957.
(9) Molchanov, A. S.; Ledenkov, S. F. *Russ. J. Phys. Chem.* **2009**, *A 28*, 2028−2031.
(10) Pettit, L. D. *Pure Appl. Chem.* **1984**, *56*, 247−292.
(11) Mosset, A.; Bonnet, J. J. *Acta Crystallogr.* **1977**, *B33*, 2807−2812.
(12) Yamauchi, O.; Odani, A.; Kohzuma, T.; Masuda, H.; Toriumi, K.; Sato, K. *Inorg. Chem.* **1989**, *28*, 4066−4068.
(13) Yamauchi, O.; Odani, A.; Masuda, H. *Inorg. Chim. Acta* **1992**, *198*, 749−761.
(14) Hamalainen, R.; Ahlgren, M.; Turpeinen, U.; Rantala, M. *Acta Chem. Scand. A* **1978**, *32*, 235.
(15) Liu, W.; Song, Y.; Li, Y.; Zou, Y.; Dang, D.; Ni, Ch.; Meng, Q. *Chem. Commun.* **2004**, *20*, 2348−2349.
(16) Yugeng, Z.; Jianmin, L. *Cryst. Res. Technol.* **1993**, *28*, 1135−1138.
(17) Majid, S.; El Rhazi, M.; Amine, A.; Brett, Ch. M. A. *Anal. Chim. Acta* **2002**, *464*, 123−133.
(18) Wojciechowska, A.; Daszkiewicz, M.; Bienko, A. *Polyhedron* **2009**, *28*, 1481−1489.
(19) Zhang, S.; Hu, N.-H. *Acta Crystallogr.* **2009**, *C 65*, m7−m9.
(20) Weng, J.; Hong, M.; Shi, Q.; Cao, R.; Chan, A. S. C. *Eur. Inorg. Chem.* **2002**, 2553−2556.
(21) (a) Apfelbaum-Tibika, F.; Bino, A. *Inorg. Chem.* **1984**, *23*, 2902−2905. (b) Franks, W. A.; Van der Helm, D. *Acta Crystallogr., Sect. B* **1971**, *27*, 1299−1310.
(22) Ye, Q.; Li, Y.-H.; Wu, Q.; Song, Y.-M.; Wang, J.-X.; Zhao, H.; Xiong, R.-G.; Xue, Z. *Chem.—Eur. J.* **2005**, *11*, 988−994.
(23) Facchin, G.; Torre, M. H. T.; Kremer, E.; Piro, O. E.; Castellano, E. E.; Baran, E. J. *J. Inorg. Biochem.* **2002**, *89*, 174−180.
(24) Wang, R.; Zheng, Z.; Jin, T.; Staples, R. J. *Angew. Chem., Int. Ed.* **1999**, *38*, 1813−1815.
(25) Li, D. Q.; Zhou, J.; Liu, X. *Acta Crystallogr.* **2007**, *C63*, m371−373.
(26) Sagiyan, A. S.; Babayan, E. E.; Geolchanyan, A. V.; Oganesyan, A. M.; Pripadchev, D. A.; Maleev, V. I. *Armenian Chem. J.* **2007**, *60*, 61.
(27) Garnier, A.; Tosi, L. *J. Inorg. Biochem.* **1979**, *10*, 147−158.
(28) Wojciechowska, A.; Daszkiewicz, M.; Staszak, Z.; Trusz-Zdybek, A.; Bienko, A.; Ozarowski, A. *Inorg. Chem.* **2011**, *50*, 11532−11542.
(29) Refat, M. S.; El-Korashy, S. A.; Ahmed, A. S. *J. Mol. Struct.* **2008**, *881*, 28−45.
(30) Islam, Md. R.; Islam, S. M. R.; Noman, A. S. M.; Khanam, J. A.; Ali, S. M. M.; Alam, S.; Lee, M. *Mycobiology* **2007**, *35* (1), 25−29.
(31) Redshaw, C.; Gibson, V. C.; Clegg, W.; Edwards, A. J.; Miles, B. *J. Chem. Soc., Dalton Trans.* **1997**, 3343−3347.
(32) (a) Mathews, I. I.; Joy, P. A.; Vasudevan, S.; Manohar, H. *Inorg. Chem.* **1991**, *30*, 2181−2185. (b) Mathews, I. I.; Manohar, H. *Polyhedron* **1991**, *10*, 2163−2169. (c) Van der Helm, D.; Ealick, S. E.;

Burks, J. E. *Acta Crystallogr., Sect. B* **1975**, *31*, 1013. (d) Novokmet, S.; Heinemann, F. W.; Zahl, A.; Alsfasser, R. *Inorg. Chem.* **2005**, *44*, 4796−4805. (e) Zhang, S.; Hu, N.-H. *Acta Crystallogr., Sect. C* **2009**, *65*, m7−m9.
(33) Van der Helm, D.; Tatsch, C. E. *Acta Crystallogr., Sect. B* **1972**, *28*, 2307.
(34) Jarzab, T. C.; Hare, C. R.; Langs, D. A. *Cryst. Struct. Commun.* **1973**, *2*, 399.
(35) Sabat, M.; Jezowska, M.; Kozlowski, H. *Inorg. Chim. Acta* **1979**, *37*, L511−L512.
(36) Vornefeld, M.; Huber, F.; Preut, H.; Ruisi, G.; Barbieri, R. *Appl. Organomet. Chem.* **1992**, *6*, 75−82.
(37) Frade, R. F. M.; Candeias, N. R.; Duarte, C. M. M.; Andre, V.; Duarte, M. T.; Gois, P. M. P.; Afonso, C. A. M. *Bioorg. Med. Chem. Lett.* **2010**, *20*, 3214−3415.
(38) Pradeep, C. P.; Supriya, S.; Zacharias, P. S.; Das, S. K. *Polyhedron* **2006**, *25*, 3588−3592.
(39) Friedma, S.; Ts'o, P. O. P. *Biochemistry* **1971**, *10*, 3099−3104.
(40) Stanell, R. M.; Li, H. J. *Biopolymers* **1974**, *13*, 1909−1926.
(41) Sheron, A.; Sharma, G.; First, E. C. *J. Biol. Chem.* **2008**, *283*, 12960−12970.
(42) (a) Yang, V.; Wang, Y.; Yang, G. *Biometals* **2011**, *24*, 737−745. (b) Yang, Ch.-T.; Vetrichelvan, M.; Yang, X.; Moubaraki, B.; Murray, K. S.; Vittal, J. J. *Dalton Trans.* **2004**, 113−121.
(43) Chen, J.; Ren, X.; Le, X.; Feng, X. *Chin. J. Chem.* **2010**, *28*, 2179−87.
(44) Zhang, F.; Yajima, T.; Masuda, H.; Odani, A.; Yamauchi, O. *Inorg. Chem.* **1997**, *36*, 5777−5784.
(45) Zhang, F.; Odani, A.; Masuda, H.; Yamauchi, O. *Inorg. Chem.* **1996**, *35*, 7148−7155.
(46) Reddy, P. R.; Manjula, P. *Chem. Biodiversity* **2009**, *6*, 71−78.
(47) Mital, R.; Sirvastava, T. S. *J. Inorg. Biochem.* **1990**, *40*, 111−120.
(48) Ou, G.-Ch.; Jiang, L.; Feng, X.-L.; Lu, T.-B. *Inorg. Chem.* **2008**, *47*, 2710−2718.
(49) (a) Shvelashvili, A. E.; Zedelashvili, E. N.; Beshkenadze, I. A.; Svanidze, O. P.; Miminoshvili, E. B.; Koberidze, N. A. *Comm. Acad. Sci. Georgia* **1984**, *116*, 521. (b) Bandyopadhyay, S.; Mukherjee, G. N.; Drew, M. G. B. *Inorg. Chim. Acta* **2006**, *359*, 3243−3251.
(50) (a) Xie, Y.; Yan, Y.; Wu, H.-H.; Yong, G.-P.; Cui, Y.; Wang, Z.-Y.; Pan, L.; Li, J.; Fan, R.; Li, R.-P.; Tian, Y.-Ch.; Pan, G.-Q.; Sheng, L.-S.; Li, X. *Inorg. Chim. Acta* **2007**, *360*, 1669−1674. (b) Wang, J.; Xu, X.; Ma, W.; Lu, L.; Yang, X. *Acta Crystallogr., Sect. E* **2007**, *E63*, m2867−m2868. (c) Rodriguez, M. L.; Ruiz-Perez, C.; Rodriguez-Romero, F. V.; Palacios, M. S.; Martin-Zarza, P. *Acta Crystallogr., Sect. C* **1990**, *46*, 1414−1416. (d) New, S. Y.; Wu, X.; Bai, S.-Q.; Koh, L. L.; Hor, T. S. A.; Xue, F. *CrystEngComm* **2011**, *13*, 4228−4235. (e) Wang, J.; Zhou, S.; Lin, D.; Ding, X.; Jiang, H.; Liu, H. *CrystEngComm* **2011**, *47*, 8355.
(51) (a) Dan, M.; Rao, C. N. R. *Chem.—Eur. J.* **2005**, *11*, 7102−7109. (b) Fleck, M.; Bohaty, L. *Acta Crystallogr.* **2004**, *C60*, m291−m295. (c) Fleck, M.; Bohaty, L. *Acta Crystallogr.* **2004**, *C61*, m412−m416. (d) Niklas, N.; Wolf, S.; Liehr, G.; Anson, Ch. E.; Powell, A. K.; Alsfasser, R. *Inorg. Chim. Acta* **2001**, *314*, 126−132. (e) Wang, S.-N.; Bai, J.; Li, Y.-Z.; Pan, Y.; Scheer, M.; You, X.-Z. *CrystEngComm* **2007**, *9*, 1084−1095. (e) Fleck, M.; Bohaty, L. *Acta Crystallogr.* **2004**, *C61*, m1890−m1893. (f) Gu, X.; Ndungu, J. M.; Qiu, W.; Ying, J.; Carducci, M. D.; Wooden, H.; Hurby, V. J. *Terahedron* **2004**, *60*, 8233−8243. (g) Menaube, L.; Saladini, M. *J. Crystollgr. Spectrosc. Res.* **1992**, *22*, 713−719.
(52) (a) Weng, J.; Hong, M.-Ch.; Cao, R.; Shi, Q.; Chan, S. C. *Chin. J. Struct. Chem.* **2003**, *22*, 195. (b) Khatib, A.; Aqra, F. *Trans. Met. Chem.* **2009**, *34*, 787−790. (c) Sahoo, S. C.; Dubey, M.; Alam, Md. A.; Ray, M. *Inorg. Chim. Acta* **2010**, *363*, 3055−3060. (d) Cai, J.; Hu, X.; Bernal, I.; Ji, L.-N. *Polyhedron* **2002**, *21*, 817−823. (e) Wang, L.; Cai, J.; Mao, Z.-W.; Feng, X.-L.; Huang, J.-W. *Trans. Met. Chem.* **2004**, *29*, 411−418. (f) Ebner, S. R.; Helland, B. J.; Jacobson, R. A.; Angelici, R. J. *Inorg. Chem.* **1980**, *19*, 175−180. (g) Mostad, A.; Natarajan, S. *Z. Kristallogr.* **1987**, *178*, 263.
(53) (a) Patra, A. K.; Chakravarty, A. R. *Proc. Indian Natl. Sci. Acad.* **2007**, *73*, 157. (b) Lindeman, S. V.; Timofeeva, T. V.; Maleyev, V. I.; Belokon, Yu. N.; Ryzhov, M. G.; Belikov, V. M.; Struchkov, Yu. T. *Acta Crystallogr., Sect. C* **1985**, *41*, 1290−1295. (c) Bian, H.-D.; Zhang, X.-Q.; Yang, X.-E.; Yu, Q.; Liang, H. *Acta Crystallogr.* **2005**, *E61*, m2237−m2239. (d) Capasso, S.; Giordano, F.; Mattia, C.; Mazzarella, L.; Ripamonti, A. *J. Chem. Soc., Dalton Trans.* **1974**, 2228−2233. (e) Peng, Q.-L.; Zhao, G.-Q.; Chen, L.-H.; Xue, L.-W. *Acta Crystallogr., Sect. E* **2010**, *66*, m1127−m1128. (f) Soloshonok, V. A.; Ellis, T. K.; Ueki, H.; Ono, T. *J. Am. Chem. Soc.* **2009**, *131*, 7208−7209.
(54) Ou, G.-Ch.; Feng, X.-L.; Lu, T.-B. *Cryst. Growth Des.* **2011**, *11*, 851−856.
(55) Muir, J. A.; Ortiz, A. *J. Appl. Crystallogr.* **1977**, *10*, 489.
(56) CSD, version 5.31: Bruno, I. J.; Cole, J. C.; Edgington, P. R.; Kessler, M.; Macrae, C. F.; McCabe, P.; Pearson, J.; Taylor, R. *Acta Crystallogr.* **2002**, *B58*, 389−397.
(57) Skoulika, S.; Michaelides, A.; Aubry, A. *Acta Crystallogr.* **1995**, *C51*, 843−846.
(58) Antolini, L.; Marcotrigiano, G.; Menabue, L.; Pellacani, G. C.; Saladini, M.; Sola, M. *Inorg. Chem.* **1985**, *24*, 3621−3626.
(59) Zhang, S.; Zhou, J. *J. Coord. Chem.* **2008**, *61*, 2488−2498.
(60) Patra, A. K.; Chakravarty, A. R. *Proc. Indian Natl. Sci. Acad.* **2007**, *73*, 37−46.
(61) Le, X.; Zhou, X.; Huang, Ch.; Feng, X. *J. Coord. Chem.* **2003**, *56*, 861−867.
(62) Patra, A. K.; Bhowmick, T.; Ramakumar, S.; Chakravarty, A. R. *Inorg. Chem.* **2007**, *46*, 9030−9032.
(63) Mizutani, M.; Tomosue, S.; Kinoshita, H.; Jitsukawa, K.; Masuda, H.; Einaga, H. *Bull. Chem. Soc. Jpn.* **1999**, *72*, 981−988.
(64) Selvakumar, P. M.; Suresh, E.; Subramanian, P. S. *Polyhedron* **2009**, *28*, 245−252.
(65) Sugimori, T.; Masuda, H.; Ohata, N.; Koiwai, K.; Odani, A.; Yamauchi, O. *Inorg. Chem.* **1997**, *36*, 576−583.
(66) *CrysAlisCCD and CrysAlisRED: CrysAlis171*, version 1.171.33.42, release 29-05-2009; Oxford Diffraction Ltd.: Oxford, U.K., 2009.
(67) Sheldrick, G. M. *Acta Crystallogr.* **2008**, *A64*, 112−122.
(68) Flack, H. D. *Acta Crystallogr.* **1983**, *A39*, 876−881.
(69) Bierman, G.; Ziegler, H. *Anal. Chem.* **1986**, *58*, 536−539.
(70) Myrczek, J. *Spectrosc. Lett.* **1990**, *23*, 1027−1039.
(71) Wojciechowska, A.; Staszak, Z.; Pietraszko, A.; Bronowska, W.; Cieślak-Golonka, M. *Polyhedron* **2001**, *21*, 2063−2073.
(72) Slavic, I. A. *Nucl. Instrum. Methods* **1976**, *134*, 285−289.
(73) Bartecki, A.; Staszak, Z. *Comput. Enhanced Spectrosc.* **1984**, *2*, 129−134.
(74) Hassan, A. K.; Pardi, L. A.; Krzystek, J.; Sienkiewicz, A.; Goy, P.; Rohrer, M.; Brunel, L.-C. *J. Magn. Reson.* **2000**, *142*, 300−312.
(75) Wojciechowska, A.; Gągor, A.; Wysokiński, R.; Trusz-Zdybek, A. *J. Inorg. Biochem.* **2012**, *117*, 93−102.
(76) Lever, A. B. P *Inorganic Electronic Spectroscopy*; Elsevier: New York, 1984.
(77) Gonzalez, E.; Rodrigue-Witchel, A.; Reber, Ch. *Coord. Chem. Rev.* **2007**, *251*, 351−363.
(78) Griend, D. A. V.; Bediako, D. K.; DeVries, M. J.; DeJong, N. A.; Heerinha, L. P. *Inorg. Chem.* **2008**, *47*, 656−662.
(79) Bertini, I.; Gatteschi, D.; Scozzafava, A. *Inorg. Chem.* **1976**, *15*, 203−207.
(80) Mohamadou, A.; Jubert, C.; Gruber, N.; Barbier, J. P. *Eur. J. Inorg. Chem.* **2004**, 1285−1291.
(81) Fereday, R. J.; Hathaway, B. J. *J. Chem. Soc., Dalton Trans.* **1972**, 197−199.
(82) Shankle, G. E.; Bates, J. B. *J. Chem. Phys.* **1976**, *64*, 2539−2548.
(83) Wang, S.-J.; Kung, X.-Y.; Duan, M.-L.; Zhang, C.-X.; Lu, Ch. *Phys. Status Solidi B* **2010**, *247*, 416−421.
(84) Yang, Z.-Y.; Wei, Q. *Physica* **2005**, *B 370*, 137−145.
(85) Gerloch, M *Magnetism and Ligand-Field Analysis*; Cambridge University Press: Cambridge, U.K., 1983.
(86) Gerloch, M.; McMeeking, R. F. *J. Chem. Soc., Dalton Trans.* **1975**, 2443−2451.
(87) Boča, R. *Struct. Bonding (Berlin)* **2006**, *117*, 1−264.

(88) Rogez, G.; Rebilly, J.-N.; Barra, A.-L.; Sorace, L.; Blondin, G.; Kirchner, N.; Duran, M.; Van Slageren, J.; Parsons, S.; Ricard, L.; Marvilliers, A.; Mallah, T. *Angew. Chem., Int. Ed.* **2005**, *44*, 1876−1879.
(89) Krzystek, J.; Ozarowski, A.; Telser, J. *Coord. Chem. Rev.* **2006**, *250*, 2308−2324.
(90) Ozarowski, A. *Inorg. Chem.* **2008**, *47*, 9760−9762.
(91) Ozarowski, A.; Szymanska, I. B.; Muziol, T.; Jezierska, J. *J. Am. Chem. Soc.* **2009**, *131*, 10279−10292.
(92) Figgis, B. N.; Hitchman, M. A. *Ligand Field Theory and Its Applications*; Wiley: New York, 2000.
(93) Maganas, D.; Krzystek, J.; Ferentinos, E.; Whyte, A. M.; Robertson, N.; Psycharis, V.; Terzis, A.; Neese, F.; Kyritsis, P. *Inorg. Chem.* **2012**, *51*, 7218−7231.
(94) Kahn, O. *Molecular Magnetism*: Wiley-VCH: New York, 1993.
(95) Desplanches, C.; Ruiz, E.; Rodriguez-Fortea, A.; Alvarez, S. *J. Am. Chem. Soc.* **2002**, *124*, 5197−5205.
(96) Guennic, B.; Le Amor, N. B.; Maynau, D.; Robert, V. *J. Chem. Theory Comput.* **2009**, *5*, 1506−1510.
(97) Choi, K.-Y.; Suh, I.-H.; Hong, C. P. *Inorg. Chem. Commun.* **1999**, *2*, 604−606.
(98) Ohta, H.; Harada, K.; Irie, K.; Kashino, S.; Kambe, T.; Sakane, G.; Shibahara, T.; Takamizawa, S.; Mori, W.; Nonoyama, M.; Hirotsu, M.; Kojima, M. *Chem. Lett.* **2001**, *30*, 842−843.
(99) Barea, E.; Navarro, J. A. R.; Salas, J. M.; Masciocchi, N.; Galli, S.; Sironi, A. *Inorg. Chem.* **2004**, *43*, 473−481.
(100) Cui, S.-X.; Zhao, Y.-L.; Zhang, J.-P.; Liu, Q. *J. Mol. Struct.* **2009**, *927*, 21−26.
(101) Ma, Y.; Cheng, A.-L.; Gao, E.-Q. *Dalton Trans.* **2010**, *39*, 3521−3526.
(102) Dutta, S.; Biswas, P.; Florke, U.; Nag, K. *Inorg. Chem.* **2010**, *49*, 7382−7400.
(103) Sadhukhan, D.; Ray, A.; Pilet, G.; Rizzoli, C.; Rosair, G. M.; Gómez-García, C. J.; Signorella, S.; Bellú, S.; Mitra, S. *Inorg. Chem.* **2011**, *50*, 8326−8339.
(104) Helios, K.; Duczmal, M.; Pietraszko, A.; Michalska, D. *Polyhedron* **2013**, *49*, 259−268.
(105) Stanila, A.; Braicu, C.; Stanila, S.; Pop, M. R. *Not. Bot. Horti Agrobot. Cluj-Napoca* **2011**, *39*, 124−129.